 Open Access

Iraqi Journal for Electrical and Electronic Engineering
Original Article

IJ EEE
University of Basrh College of Engineering

Vector-controlled Permanent Magnet Synchronous Motor Using Indirect Matrix Converter

Zainab M. Abed*[1], Turki K. Hassan[1]
[1]Electrical Engineering Department, Al-Mustansiriayah University
Baghdad, Iraq

Correspondence
*Zainab M. Abed
Electrical Engineering Department,
Al-Mustansiriayah University, Baghdad, Iraq
Email: zainab.mahmood21290@gmail.com

Abstract
In this paper, the vector-controlled Permanent Magnet Synchronous Motor (PMSM) fed by Indirect Matrix Converter (IMC) is analyzed, designed, and simulated by using the IMC with Carrier Based Pulse Width Modulation (CBPWM). The CBPWM strategy is based on Space Vector Pulse Width Modulation (SVPWM) analysis, it is used to enhance the input current waveform, reduce the complexity of switching signals generation, and to solve the commutation problem. The traditional PMSM drive system is simulated for comparison with proposed drive system. The proposed drive system is compared to the traditional drive system using the Total Harmonic Distortion (THD). The comparison results show that the proposed drive system outperform the traditional drive system by THD different of 1/30 of input current and 1/1.5 of stator current, with high input power factor.
KEYWORDS: Permanent Magnet Synchronous Motor, Indirect Matrix Converter, Carrier-Based PWM, Vector Control.

I. INTRODUCTION

The PMSM is commonly used nowadays, due to its light weight, wide speed range operation, small torque ripple, and low rotational inertia. It is widely used in different applications like industry, aerospace, agriculture. The motor speed can be simply controlled with vector control method [1].

The IMC is a direct AC-AC converter, it is a set of controlled switches, which connects each input to each output directly, with no need to bulky storage elements. It can provide approximately current sinusoidal waveform at the input and output, better input power factor, and allows two-direction power flow [2]. It is suitable in drive systems with variable frequency, such as aviation aircraft, wind power generation [3].

The IMC is used to feed PMSM in [3] with SVPWM and fuzzy Proportional Integral (PI) speed controller, to enhance the PI controller performance during the transient response. The authors in [4] present a method to enhance the IMC voltage transfer ratio of the PMSM drive system. The method uses SVPWM strategy to control the IMC switches, and to enhance the power factor, by regulating the terminal reactive power and generating the d-current reference value.

The authors in [5] use a CBPWM method, with fixed slope triangular signal as a carrier signal, based on SVPWM analysis. The IMC is implemented to feed three-phase RL-load by using Digital Signal Processing (DSP) and Complex Programmable Logic Device. In [6] the authors use the CBPWM method with carrier signal of symmetrical triangular, to generate rectifier

and inverter PWM signals. The IMC is implemented to feed couple three-phase RL-loads by a single three-phase power supply, to enhance the IMC maximum voltage transfer ratio.

In [7] the CBPWM method is used for three-to-five phase IMC, the CBPWM method is applied for two stages independently. The IMC is implemented to feed five-phase RL-load, by a three-phase power source using DSP controller. A voltage transfer ratio of IMC is improved by applying the over modulation mode for each stage. In [8] the authors use the CBPWM for three-to-five phase IMC, with symmetrical triangular carrier signal for IMC two stages, The IMC is implemented to feed five-phase RL-load, by three-phase power source using DSP controller and Field Programmable Gate Array.

In this paper, the CBPWM method based on SVPWM analysis, which is suggested in [5] and [8], is used to control the IMC switches of the vector controlled PMSM drive system. In addition, the proposed PMSM drive system performance is compared to traditional (AC-DC-AC) drive system.

II. THE INDIRECT MATRIX CONVERTER

The structure of IMC contains two stages, the first stage is a set of bidirectional switches form the rectifier stage, and the other stage is a set of unidirectional switches form the inverter stage, with no energy storage elements between the two stages, as shown in Fig. 1 [5].

Table 1 Switching states, duty cycles, input current, and dc-link average voltages for rectifier stage

Input voltage phase $\omega_{in}t$	Sector	ON switch	Modulated switches and duty cycles				Input current magnitude	Average dc-link voltage ($\bar{V}_{dc}$)
			d_x		d_y			
$-\pi/6 .. \pi/6$	1	S_{ap}	S_{bn}	$-v_b/v_a$	S_{cn}	$-v_c/v_a$	$2\,I_{dc}/\sqrt{3}$	$3V_{in}^2/2v_a$
$\pi/6 .. \pi/2$	2	S_{cn}	S_{bp}	$-v_b/v_c$	S_{ap}	$-v_a/v_c$	$2\,I_{dc}/\sqrt{3}$	$-3V_{in}^2/2v_c$
$\pi/2 .. 5\pi/6$	3	S_{bp}	S_{cn}	$-v_c/v_b$	S_{an}	$-v_a/v_b$	$2\,I_{dc}/\sqrt{3}$	$3V_{in}^2/2v_b$
$5\pi/6 .. 7\pi/6$	4	S_{an}	S_{cp}	$-v_c/v_a$	S_{bp}	$-v_b/v_a$	$2\,I_{dc}/\sqrt{3}$	$-3V_{in}^2/2v_a$
$7\pi/6 .. 9\pi/6$	5	S_{cp}	S_{an}	$-v_a/v_c$	S_{bn}	$-v_b/v_c$	$2\,I_{dc}/\sqrt{3}$	$3V_{in}^2/2v_c$
$9\pi/6 .. 11\pi/6$	6	S_{bn}	S_{ap}	$-v_a/v_b$	S_{cp}	$-v_c/v_b$	$2\,I_{dc}/\sqrt{3}$	$-3V_{in}^2/2v_b$

The input filter is used to enhance the sinusoidal waveform of the input current, prevent the overvoltage generation, improve the input power factor, and to reduce the switching noise [9],[10]. When a fault occurs at the load, the simple diode in series with small size capacitor, which form the clamp circuit is used to absorb the magnetic energy stored in the inductors of the input filter [11].
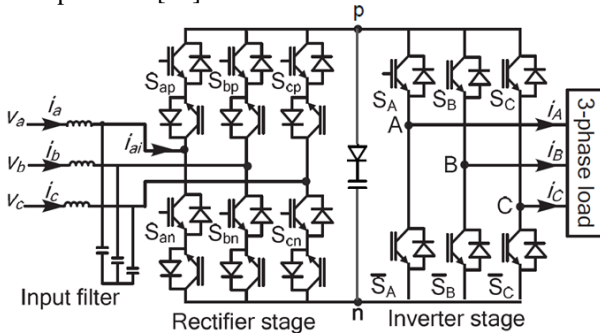

Fig. 1 Three to three phase IMC construction [5]

The SVPWM analysis of the IMC can be divided into two parts. The first is based on the reference input current space vectors analysis for the rectifier stage. The second is based on the reference output voltage space vectors analysis for the inverter stage [5], the analysis is demonstrated in the following sections.

A. Rectifier Stage SVPWM Analysis

The input phase voltages for a balanced three-phase grid, have two conditions which split into six sectors. The input phase voltages in the first condition are: one is positive and the rest are negative (sectors 1,3,5). While in the second condition, input phase voltages are: one is negative and the rest are positive (sectors 2,4,6) [5] as shown in Fig. 2.
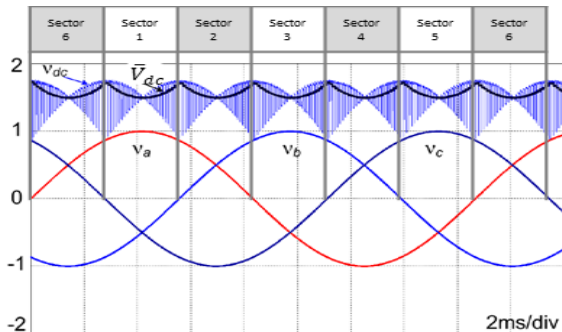

Fig. 2 Input voltage divided into six sectors and the dc-link voltage (v_{dc}) with its average value ($\bar{V}_{dc}$)

It is assumed that the three-phase grid voltages are given as:
$$v_a = V_{in} \cos(\omega_{in}t) \quad (1)$$
$$v_b = V_{in} \cos(\omega_{in}t - 2\pi/3) \quad (2)$$
$$v_c = V_{in} \cos(\omega_{in}t + 2\pi/3) \quad (3)$$
where; V_{in} and ω_{in} are represent the input phase voltage amplitude and angular frequency, respectively.

Table 1 shows the space vectors of the input current, where Idc represent the dc-link current. It is clear from the table that the current vectors have six fixed direction, as shown in Fig. 3-a.

There are two adjacent active current vectors chosen to generate the reference input current vector depending on its position. As an example, the vector of the reference input current with θ_{in} between $-\pi/6$ and $\pi/6$ laying in sector 1, is generated by two vectors Iab and Iac, where these two vectors represent the connection of input phase a positive pole, to the input phases b and c negative poles, as shown in Fig. 3-b.
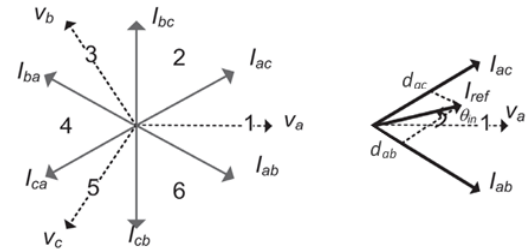

Fig. 3 The space vector diagram of the rectifier stage

The duty cycles of the two active vectors of sector 1, Iab and Iac, are given as dab and dac :
$$d_{ab} = m_r \sin(\pi/6 - \theta_{in}) \quad (4)$$
$$d_{ac} = m_r \sin(\theta_{in} + \pi/6) \quad (5)$$
and the other one is the zero vector duty cycle, which means there is no input voltage applied to dc-link voltage.
$$d_0 = 1 - d_{ab} - d_{ac} \quad (6)$$
where; m_r is the rectifier stage modulation index, and θ_{in} is the angle of the vector of the reference input current

The maximum dc-link voltage can be obtained by neglecting the zero vectors. Therefore, the switching sequence consists of two active vectors of the current, and their duty cycles are recalculated and defined as dx and dy, respectively:
$$d_x = \frac{d_{ab}}{d_{ab}+d_{ac}} = -\frac{\cos\left(\theta_{in} - \frac{2\pi}{3}\right)}{\cos(\theta_{in})} = -\frac{v_b}{v_a} \quad (7)$$

$$d_y = \frac{d_{ac}}{d_{ab}+d_{ac}} = -\frac{\cos\left(\theta_{in}+\frac{2\pi}{3}\right)}{\cos(\theta_{in})} = -\frac{v_c}{v_a} \qquad (8)$$

From equations above and for one sampling interval, the average value of the dc-link voltage is:

$$\overline{V}_{dc} = d_x v_{ab} + d_y v_{ac} = \frac{3}{2}\frac{V_{in}^2}{v_a} \qquad (9)$$

the dc-link voltage V_{dc} and $\overline{V}_{dc}$, as shown in Fig. 2, are generated by the rectifier stage control, the $\overline{V}_{dc}$ varies with six times of the input voltage frequency with respective maximum and minimum values of [5],[8]:

$$V_{dc(max)} = \sqrt{3}\, V_{in} \qquad (10)$$

$$V_{dc(min)} = \frac{3V_{in}}{2} \qquad (11)$$

Applying the same approach, duty cycles and switching states of other sectors can be obtained, and all these information are stated in table 1.

B. Inverter Stage SVPWM Analysis

The desired three-phase output voltage is symmetrical and displaced by $2\pi/3$, as follow:

$$v_A = V_{out}\cos(\omega_{out}t) \qquad (12)$$

$$v_B = V_{out}\cos(\omega_{out}t - 2\pi/3) \qquad (13)$$

$$v_C = V_{out}\cos(\omega_{out}t + 2\pi/3) \qquad (14)$$

where; V_{out} and ω_{out} represent the output phase voltage amplitude and angular frequency, respectively.
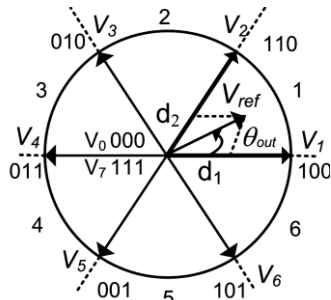

Fig. 4 Space vector diagram of three-phase inverter

The inverter with three legs has ability to produce the three-phase voltage, each leg has two switches operated in a complementary manner, resulting in 2^3 (8) internal states, where 0 and 7 states are zero vectors, and the other six states are active vectors, these vectors are distributed in six sectors, as shown in Fig. 4. For the reference output voltage V_{ref} with θ_{out} between 0 and $\pi/3$, as example, it located in sector 1, the active vectors that are used to generate this reference output voltage are V1 and V2, as shown in Fig. 4, with the following equation:

$$V_{ref} = d_1 V_1 + d_2 V_2 \qquad (15)$$

where; d_1 and d_2 are the sector 1 active vectors duty cycles and they are defined as:

$$d_1 = \frac{\sqrt{3}}{2} m_i \sin(\pi/3 - \theta_{out}) \qquad (16)$$

$$d_2 = \frac{\sqrt{3}}{2} m_i \sin(\theta_{out}) \qquad (17)$$

and the zero vectors duty cycles are:

$$d_0 = d_7 = \frac{1}{2}(1 - d_1 - d_2) \qquad (18)$$

where; θ_{out} is the reference output voltage angle, and m_i is inverter stage modulation index, it is defined as:

$$m_i = 2\frac{V_{out}}{\overline{V}_{dc}} \qquad (19)$$

and the maximum value of m_i is:

$$m_{i(max)} = \frac{1}{\cos\frac{\pi}{6}} \qquad (20)$$

The voltage transfer ratio of the three to three-phase IMC is defined as:

$$q = \frac{V_{out}}{V_{in}} \qquad (21)$$

from equations (11), (19), (20), and (21) the maximum voltage transfer ratio of the three to three-phase IMC is [8]:

$$q_{max} = \frac{3}{2}\frac{1}{2}\frac{1}{\cos\frac{\pi}{6}} = 0.866 \qquad (22)$$

C. The rectifier and inverter stages Synchronism

In one sampling interval, for rectifier stage there are two switching states, that produce two line-to-line voltages, which are converted to dc-link voltage. According to equation (9), there are two positive line-to-line input voltages, which feed the three-phase inverter. Therefore, there are two groups of the inverter stage switching states. The rectifier and inverter stages switching states should be mixed, to obtain balanced three phase input current and three-phase output voltage, and their duty cycles are produced by cross product of the both stages duty cycles, as shown in Fig. 5 for sector 1:

$$d_{1(ab)} = d_1 . d_x \; ; d_{1(ac)} = d_1 . d_y \qquad (23)$$

$$d_{2(ab)} = d_2 . d_x \; ; d_{2(ac)} = d_2 . d_y \qquad (24)$$

$$d_{0(ab)} = d_0 . d_x \; ; d_{0(ac)} = d_0 . d_y \qquad (25)$$

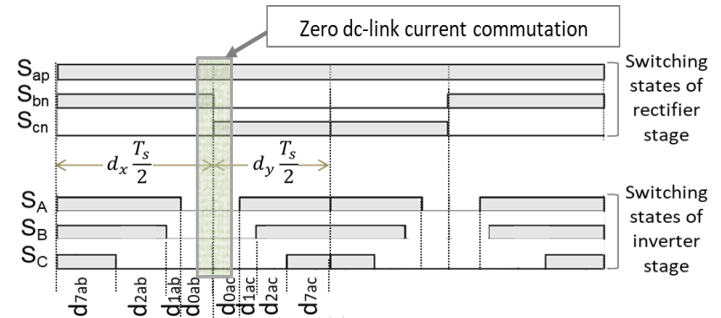$$d_{7(ab)} = d_7 . d_x \; ; d_{7(ac)} = d_7 . d_y \qquad (26)$$

Fig. 5 Switching states for rectifier and inverter switches

For commutation of zero dc-link current in rectifier stage, as shown in Fig. 5, all currents are zero in rectifier stage, due to zero vectors applied in inverter stage during the commutation. The complex multi-step commutation process can be avoided, and the rectifier stage switching losses can be minimized, due to commutation of zero dc-link current [8].

III. THE CBPWM METHOD

In the analysis of the IMC by the SVPWM method, there are two modulation methods for rectifier and inverter stages, each SVPWM needs a complex process, as a selection of effective vectors and determine their duty cycles, by calculating different equations independently for both stages, the switching states of both stages are arranged, to achieve zero dc-link current commutation and balanced output voltages. Therefore, the SVPWM needs many calculations and tables to complete the

process. In order to avoid this complex process, the CBPWM based on SVPWM analysis is developed, to generate gating pulses of switches easily for rectifier and inverter stages.

In CBPWM method, the generation of PWM signals is based on the comparison between the modulation signals and high-frequency carrier signal. The carrier signal used in generation of the PWM signals, for rectifier stage and inverter stage, is symmetrical triangular signal with fixed slope, which described by:

$$v_t = \left(\frac{4}{T_s} t - 1\right) V_{in} ; 0 \le t \le \frac{T_s}{2} \tag{27}$$

where; V_{in} is the amplitude of input phase voltage, and v_t is the instantaneous value of carrier signal.

A. Rectifier stage control

The timing and sequence of modulated switches, for the sector 1 reference input current vector, and the carrier and modulation signals, which are required to generate the PWM of the rectifier stage are shown in Fig. 6.

For half of one sampling interval, T_n the period of gating pulse of switch S_{bn} is:

$$T_n = d_x \frac{T_s}{2} \tag{28}$$

from equations (27) and (28), the rectifier stage modulation signal is obtained by:

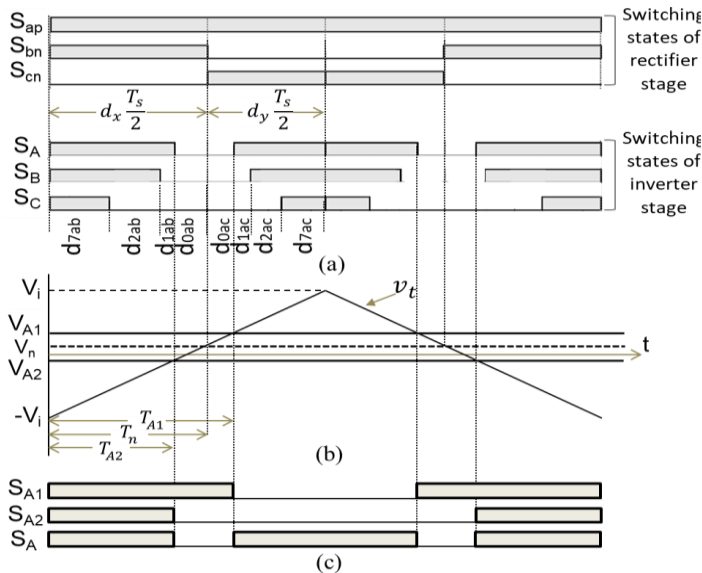$$V_n = (2d_x - 1) V_{in} \tag{29}$$

Fig. 6 Switching states and generation of PWM for rectifier and inverter switches (a) Switching states of IMC stages (b) Carrier and modulation signals (c) Gating pulses of switch A

The gating pulse of switch S_{bn} (PWM0) is obtained by intersection the modulation signal, V_n, with the carrier signal, v_t. The gating pulse of switch S_{cn} (PWM1) is the complement to switch S_{bn}. And all the other switches, S_{an}, S_{bp}, and S_{cp} are in off-state. Table 2 shows the gating pulses of rectifier swithes for six sectors.

B. Inverter stage control

In the traditional three-phase inverter fed by constant dc voltage, only three modulation signals are used, to compare with the carrier signal in one sampling interval. For IMC, there are two values of the dc-link voltage, depending on the voltages of input source. Therefore, the switching pattern of the inverter stage consists of two parts with different values, and the inverter stage switching frequency is twice of the rectifier stage switching frequency. There are two inverter stage modulation signals obtained from the duty cycles of the rectifier stage d_x and d_y, these signals are compared with respect to the carrier signal, to generate two pulses.

Table 2 The switching states of rectifier stage

Sector	S_{ap}	S_{an}	S_{bp}	S_{bn}	S_{cp}	S_{cn}
1	1	0	0	PWM0	0	PWM1
2	PWM0	0	PWM1	0	0	1
3	0	PWM1	1	0	0	PWM0
4	0	1	PWM0	0	PWM1	0
5	0	PWM0	0	PWM1	1	0
6	PWM1	0	0	1	PWM0	0

By applying the XNOR function, the upper switch gating pulse is obtained for each phase of the inverter, and the lower switch gating pulse is the complement of that the upper. In sector 1 as an example, the two modulation signals V_{A1} and V_{A2} are determined according to v_{ab} and v_{ac}, respectively, these signals are compared with respect to the carrier signal v_t, to obtain two pulses S_{A1} and S_{A2}, then the gating pulse of switch S_A is determined by:

$$S_A = S_{A1}.S_{A2} + \overline{S_{A1}}.\overline{S_{A2}} \tag{30}$$

Fig. 6 shows the generation of the gating pulse of upper switch of phase-A, the durations T_{A1} and T_{A2} can be written according to equations (23-26) as follows:

$$T_{A1} = (d_{7(ab)} + d_{1(ab)} + d_{2(ab)} + d_{0(ab)} + d_{0(ac)})\frac{T_s}{2} = (d_x + d_{0(ac)})\frac{T_s}{2} \tag{31}$$

$$T_{A2} = \left(d_{7(ab)} + d_{1(ab)} + d_{2(ab)}\right)\frac{T_s}{2} = (d_x - d_{0(ab)})\frac{T_s}{2} \tag{32}$$

by substituting the above equations into equation (27), the two modulation signals V_{A1} and V_{A2} are:

$$v_{A1} = \left(-2d_y \frac{v_A + v_{offset}}{\bar{V}_{dc}} + d_x\right) V_{in} \tag{33}$$

$$v_{A2} = \left(2d_x \frac{v_A + v_{offset}}{\bar{V}_{dc}} - d_y\right) V_{in} \tag{34}$$

where; v_{offset} is the offset voltage and is given as:

$$v_{offset} = -\frac{1}{2}(v_A + v_C) \tag{35}$$

the three equations (33-35) are obtained for reference output voltage located in sector 1. These equations can be generalized, to be applied for other reference output voltages, which are located in any sector, to obtain the switch S_X modulation signals (X: A, B, C) of inverter stage, as follows:

$$v_{X1} = \left(-2d_y \frac{v_X + v_{offset}}{\bar{V}_{dc}} + d_x\right) V_{in} \tag{36}$$

$$v_{X2} = \left(2d_x \frac{v_X + v_{offset}}{\bar{V}_{dc}} - d_y\right) V_{in} \tag{37}$$

$$v_{offset} = -\frac{1}{2}(v_{max} + v_{min}) \tag{38}$$

where; v_x is the fundamental output phase voltage, v_{max} is the maximum value of (v_A, v_B, v_C), and v_{min} is the minimum value of (v_A, v_B, v_C).

Fig. 7 shows the block diagram of the CBPWM for the two stages of the IMC. The performance of this modulation method is the same of SVPWM method, because it is based on the

mathematical analysis of SVPWM, which is clear in the relationship between the offset voltage in CBPWM and distribution of zero vectors in SVPWM [6],[8],[5].

$$T_e = \frac{3}{2}\frac{p}{2}(\lambda_d i_q - \lambda_q i_d) \qquad (43)$$

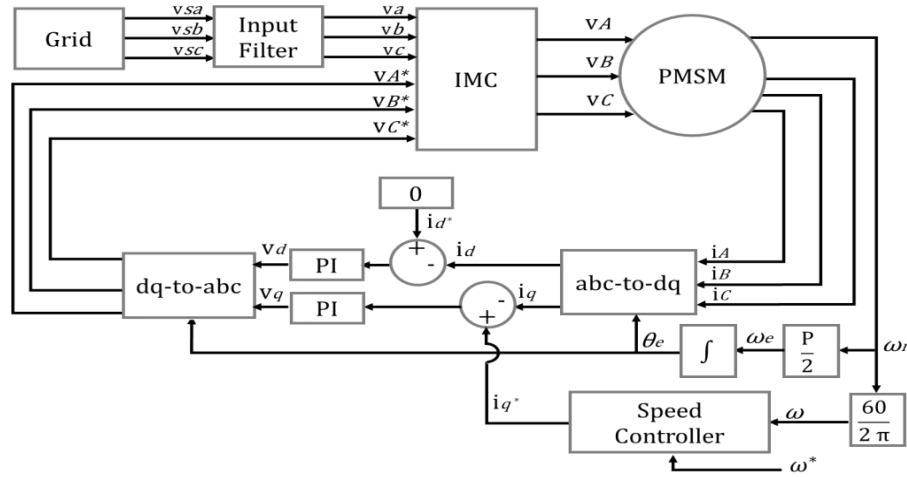where; v_d and v_q are the stator voltages in d and q axis, i_d and
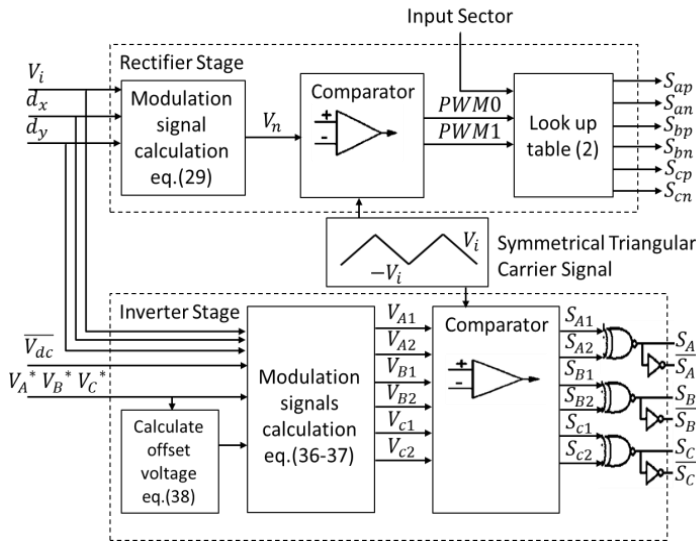

Fig. 8 Block diagram of PMSM drive system

Fig. 7 Block diagram of the CBPWM method

IV. THE PMSM MODELING

The permanent magnets with high performance and residual flux, gives a superior performance to the permanent magnet motors over the other AC motor types [12]. The PMSM characteristics are wide speed range, light weight, small size, low rotational inertia, and the torque ripple is lower than the induction motor and traditional synchronous motor, which gives it the superior in high-performance applications [1]. The model of three-phase PMSM can be explained in the following equations [13]:

$$v_d = R_s i_d + \frac{d\lambda_d}{dt} - \omega_e \lambda_q \qquad (39)$$

$$v_q = R_s i_q + \frac{d\lambda_q}{dt} + \omega_e \lambda_d \qquad (40)$$

$$\lambda_d = L_d i_d + \lambda_m \qquad (41)$$

$$\lambda_q = L_q i_q \qquad (42)$$

i_q are the stator currents in d and q axis, λ_d and λ_q are the stator fluxes in d and q axis, L_d and L_q are the winding inductances in d and q axis, λ_m is the amplitude of permanent magnet flux linkage, R_s is the stator resistance, p is the number of poles, ω_e is the electrical speed in rad/s.

The Mechanical motion equation is given by:

$$T_e = T_L + J\frac{d\omega_r}{dt} + B\omega_r \qquad (44)$$

where; T_e and T_L are the electromagnetic torque (developed torque) and load torque, J and B are the inertia moment and friction factor, and ω_r is the mechanical speed in rad/s. With assumption that $L_d \approx L_q$ to get maximum torque and maximum efficiency, the developed torque is [13], [1]:

$$T_e = \frac{3}{2}\frac{p}{2}\lambda_m i_q \qquad (45)$$

where; p and λ_m are constant values for the unique motor, while i_q is the only variable in equation above. Therefore, it is possible to control the torque as a function of i_q .

In vector control method, the three-phase motor currents (a-b-c) are decoupled, by transforming there to two-phase currents (d-q), which represent the flux producing and torque components of stator current, respectively [14].

$$\begin{bmatrix} i_d \\ i_q \end{bmatrix} = \frac{2}{3}\begin{bmatrix} \cos\theta & \cos(\theta-\alpha) & \cos(\theta-2\alpha) \\ -\sin\theta & -\sin(\theta-\alpha) & -\sin(\theta-2\alpha) \end{bmatrix}\begin{bmatrix} i_A \\ i_B \\ i_C \end{bmatrix} \quad (46)$$

where; θ is the rotor angle and α=2π/3.

The (d-q) currents are independently compared with their reference currents, then controlled with PI controllers, to achieve the (d-q) voltages. The (d-q) voltages are transformed back to (a-b-c) reference output voltages, which are utilized to control the IMC switches, the reference q current is a function of the speed error and the reference of d current is set to zero [1]. The speed error is calculated, by comparing the speed of the motor with the reference speed, and then it is controlled by the PI controller, to produce the reference q current [14]. Fig. 8 shows the block diagram of the complete PMSM drive system.

In this paper, the implementation of the PMSM drive system by using MATLAB/Simulink as shown in Fig. 9. The flowchart of complete Simulink model is shown in appendix-A. The
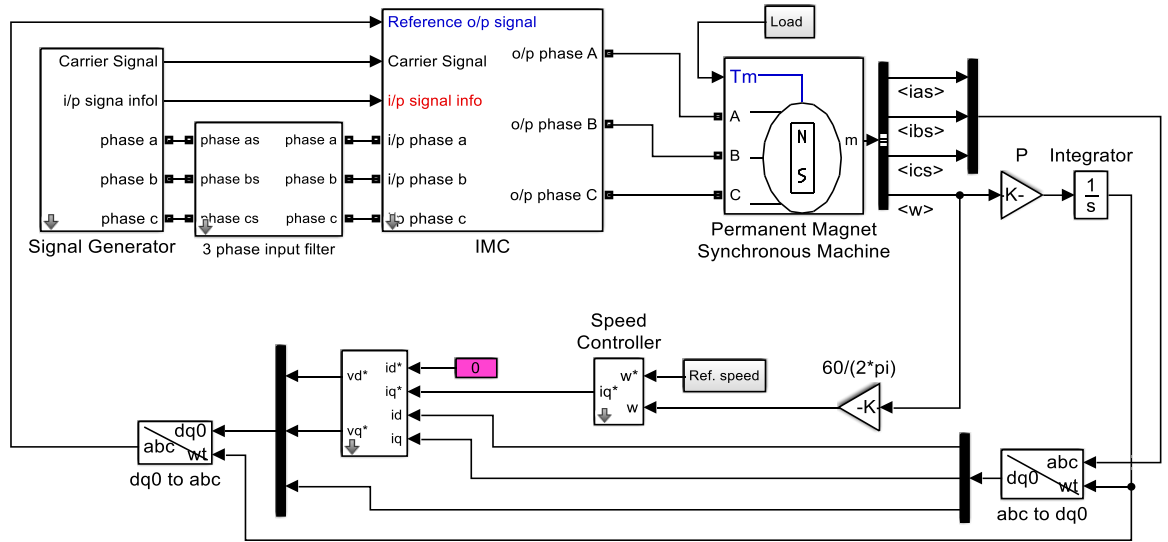
V. SIMULATION RESULTS

Fig. 9 Simulink model of the proposed system

Table 3 The PMSM drive system parameters

Parameters	Data
Three-phase input supply	voltage amplitude 220V, f=50 Hz
Input filter	C_f=2μF, L_f=2.85mH
Carrier signal	220 V, f=5 kHz
Parameters of motor [3]	R_s=0.9585Ω, L_d= L_q =5.25mH, Pole pairs=4, Full load=6N.m flux linkage= 0.1827Wb, J=6329x10^{-7} kg.m^2, B=3035x10^{-7} N.m.s
PI controllers parameters	Speed controller: k_{ps}=0.25, k_{is}=1.4 d-current controller: k_{pd}=1, k_{id}=25, q-current controller: k_{pq}=1, k_{iq}=25
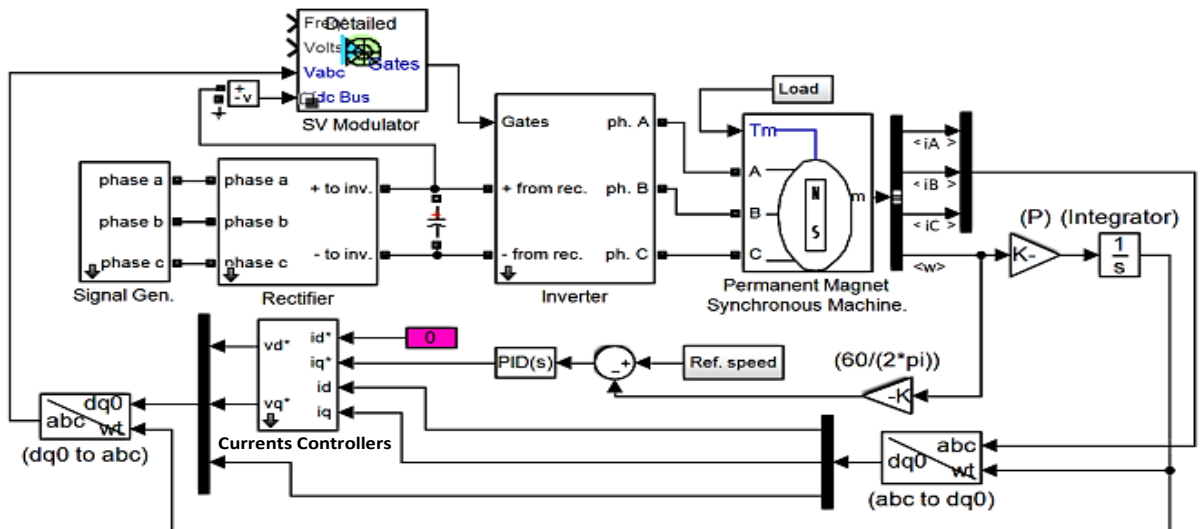
Fig. 10 Simulink model of traditional PMSM drive system

PMSM is simulated by using *Permanent Magnet Synchronous*

Machine block, this block is used in motor mode, three-phase sinusoidal model.

The parameters of the PMSM and other drive sys-tem components are stated in table 3.

Fig. 10 shows the Simulink model of traditional PMSM drive system, with SVPWM to control the inverter switches. This system is used to compare with the performance of the proposed drive system. This comparison is concentrated about the

performance of the converters, including input and output current waveforms, THD, and the input power factor.

The traditional system is tested under fixed speed with variable load, the speed is set at 750 r.p.m. The load is increased from 2 to 4N.m and from 4 to 6N.m at times of 4 and 6.5 second, respectively.
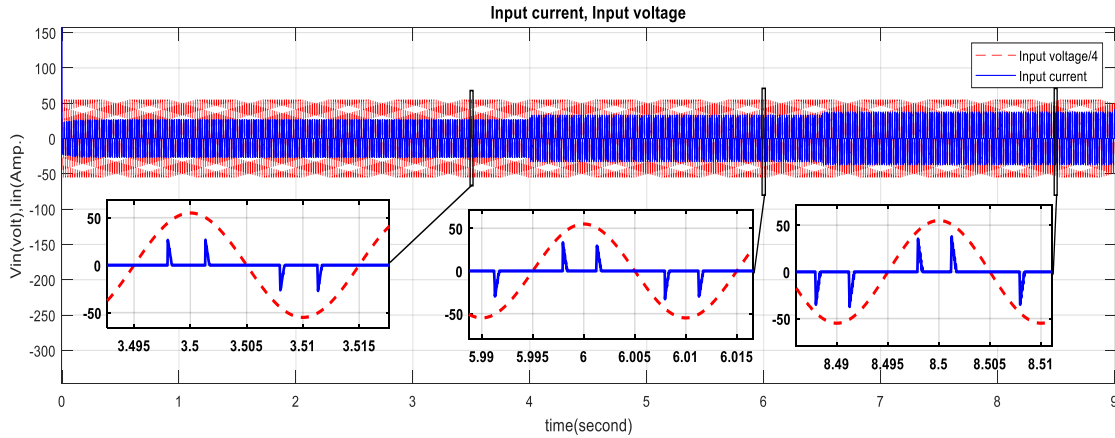
Fig. 11 The phase-a input current and voltage of traditional drive system under variable load operation
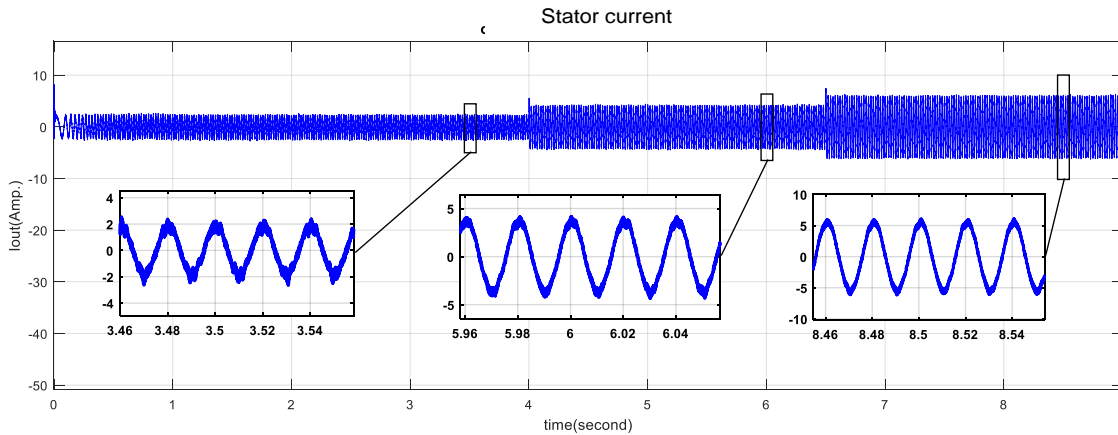
Fig. 12 The phase-A stator current of traditional drive system under variable load operation
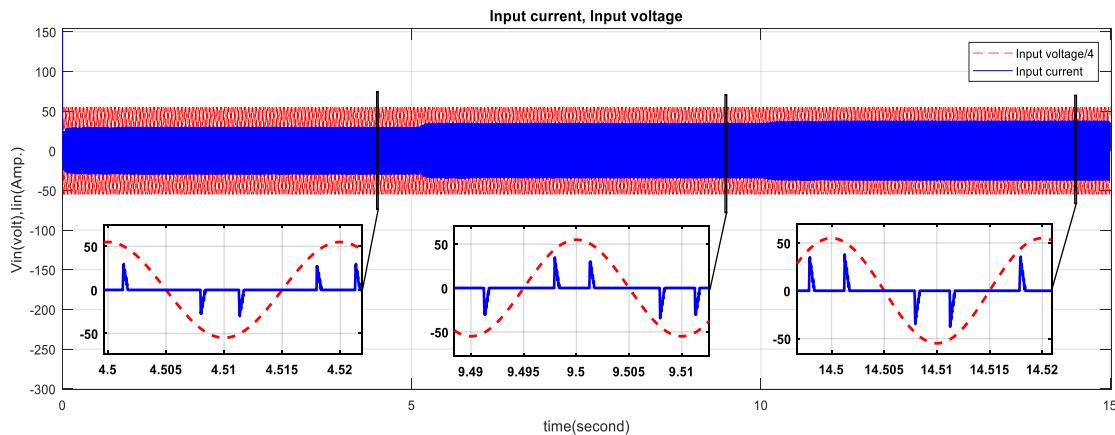

Fig. 13 The phase-a input current and voltage of traditional drive system under fixed load operation

The input current waveform is shown in Fig. 11, the commutation of phases causes high distortion to the input current with THD of 326.99%, 305.54%, and 289.41% for loads of 2, 4, and 6N.m, respectively. The stator current waveform in Fig. 12 has a THD of 16.34%, 8.45%, and 5.77% for loads of 2, 4, and 6N.m, respectively.

This system is tested again under fixed load with variable speed, the load is set at 6N.m with speed is 250 r.p.m, then the speed is increased to 500 r.p.m at time of 5 second, and then it is increased to 750 r.p.m at time of 10 second.

The input current waveform is shown in Fig. 13, the THD of the input current is 321.83%, 303.55%, and 289.41% for speeds
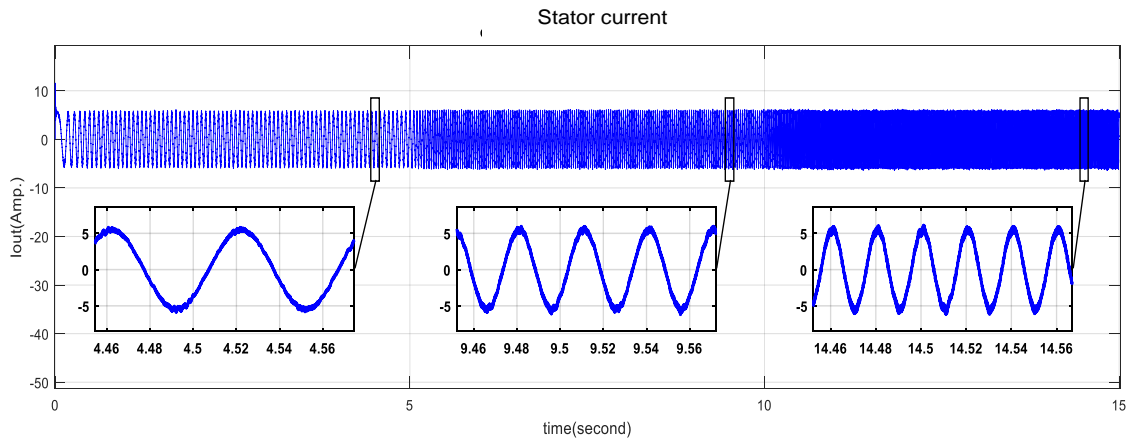

Fig. 14 The phase-A stator current of traditional drive system under fixed load operation
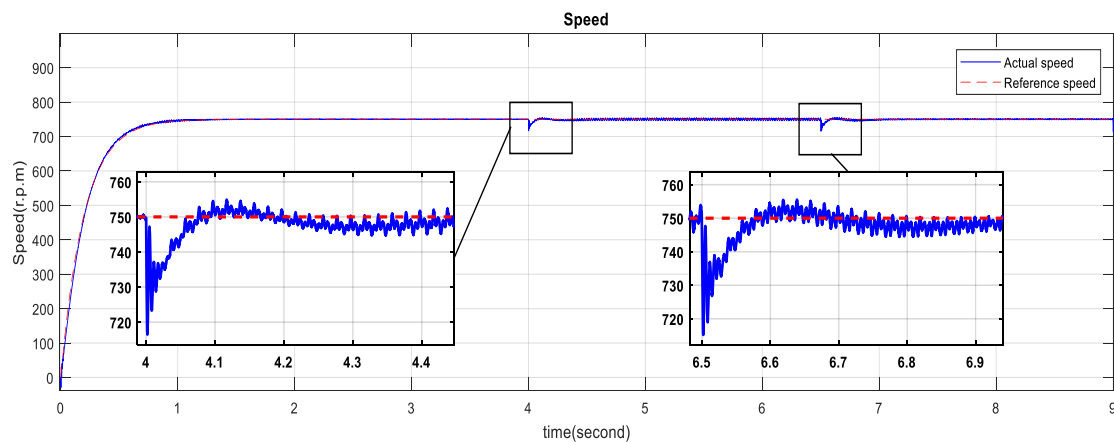

Fig. 15 The speed response of the proposed drive system under variable load operation
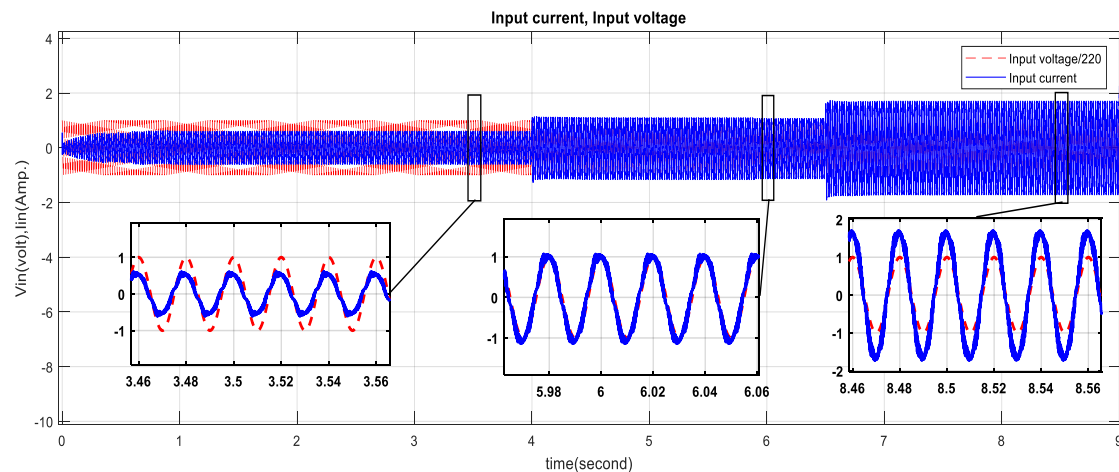

Fig. 16 The phase-a input current and voltage of the proposed drive system under variable load operation

of 250, 500, and 750 r.p.m, respectively. The stator current waveform in Fig. 14 has a THD of 3.15%, 4.56% and 5.77% speeds of 250, 500, and 750 r.p.m, respectively.

The proposed system is tested under fixed speed with variable load, the speed is set at 750 r.p.m, the rising of speed response in Fig. 15 is identical to the reference speed. The load is increased from 2 to 4N.m and from 4 to 6N.m at times of 4 and 6.5 second, respectively, the speed response shows disturbance with downshoot of 4.4667% and 4.6667%, overshoot of 0.6667% and 0.7333%, respectively, and stabilizes after 0.55 second for both, the peck-to-peak steady state ripple in speed is seen to be 0.1520%, 1.0667%, and 0.3400% for loads of 2, 4, and 6 N.m, respectively.

The input current waveform is shown in Fig. 16 using of the IMC improves the input current waveform. The input current is approximately sinusoidal waveform with small distortion, the phase shift between the input current and voltage is very small. The THD of the input current is 10.83%, 10.21%, and 9.77% with input power factor of 0.9704, 0.9930, and 0.9949 for loads of 2, 4, and 6N.m, respectively. The stator current waveform is shown in Fig. 17, it has a THD of 10.04%, 6.09%, and 3.56% for loads of 2, 4, and 6N.m, respectively.

This system is tested again under fixed load with variable speed. The load is set at 6N.m with speed is 250 r.p.m, then the speed is increased to 500 r.p.m at time of 5 second, and then it is increased to 750 r.p.m at time of 10 second.
The rising of speed response in Fig. 18 is identical to the reference speed at all speeds. The peck-to-peak steady state ripple in speed is seen to be 0.1200%, 0.2800%, and 0.3400% for speeds of 250, 500, and 750 r.p.m, respectively.

The input current waveform is shown in Fig. 19, the THD of the input current is 10.68%, 10.12%, and 9.77% with input power factor of 0.9799, 0.9948, and 0.9949 for speeds of 250, 500, and 750 r.p.m, respectively. The stator current waveform is shown in Fig. 20, it has a THD of 1.68%, 3.46%, and 3.56% for speeds of 250, 500, and 750 r.p.m, respectively.

VI. CONCLUSIONS

The performance of IMC for proposed PMSM drive system is compared with the performance of the traditional AC-DC-AC converter and the following conclusions are outcome:
1. The IMC enhances the input current waveform and reduces the THD. The current waveform is closed to sinusoidal waveform, with THD less than 11%.
2. As comparison, the THD of the input current by using IMC, is approximately 1/30 of it, by using traditional converter, under the same operation conditions.
3. The input power factor by using the IMC is approximated to be unity.
4. The CBPWM method reduces the complexity of the SVPWM method, and solves the commutation problem, by suitable dealing with zero-vectors, depending on SVPWM analysis.

CONFLICT OF INTEREST

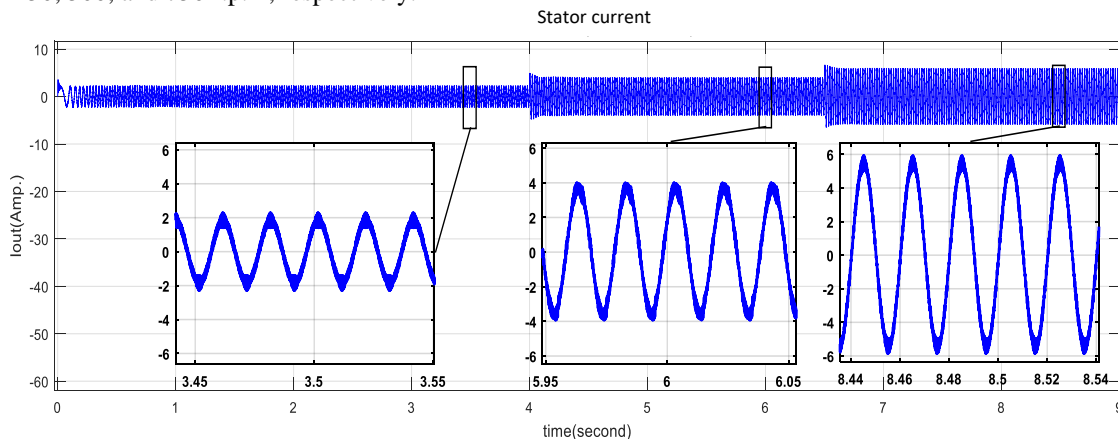The authors have no conflict of relevant interest to this article.

Fig. 17 The phase-A stator current of the proposed drive system under variable load operation
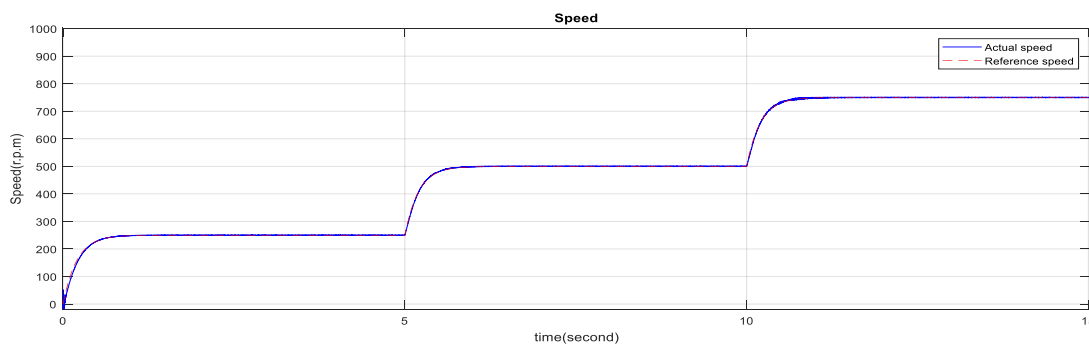

Fig. 18 The speed response of the proposed drive system under fixed load operation
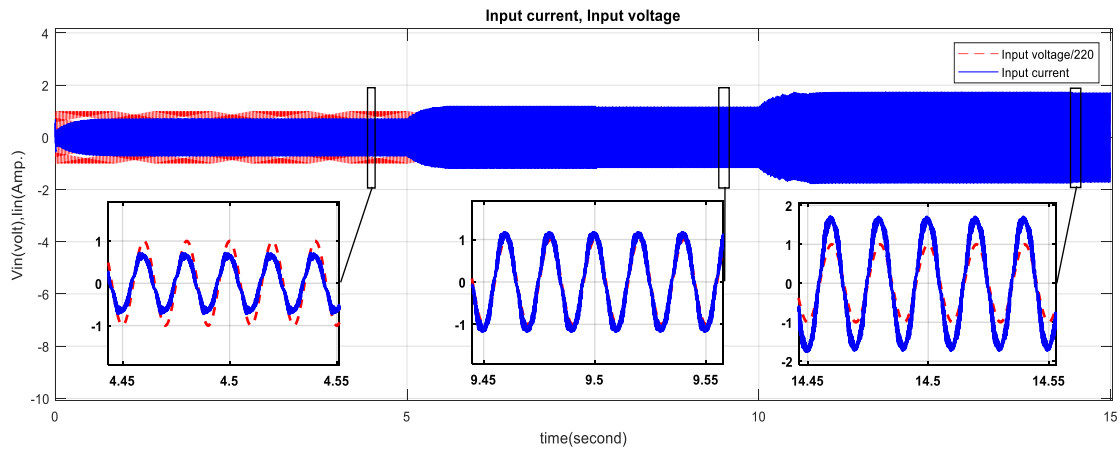
Fig. 19 The phase-a input current and voltage of the IMC-PI drive system under fixed load operation
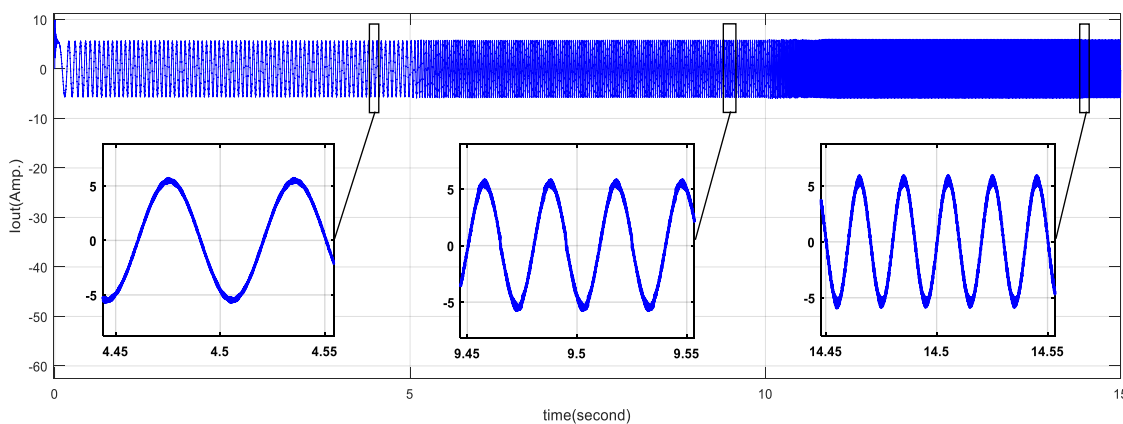

Fig. 20 The phase-A stator current of the IMC-PI drive system under fixed load operation

REFERENCES

[1] Y. Zhou, W. Shang, M. Liu, X. Li, and Y. Zeng. *Simulation of PMSM Vector Control Based on a Self-tuning Fuzzy PI Controller*. 8th International Conference on Biomedical Engineering and Informatics (BMEI), p.p 609 – 613, 2015.

[2] L. Zarri. Control of Matrix Converters. Ph.D thesis, Department of Electrical Engineering, University of Bologna, 2007.

[3] S. Lishan, P. Xiao, and L. Hongchen. *IMC fed PMSM control system based on fuzzy PI*. IEEE International Conference on Computer Science and Automation Engineering, Vol. 3, p.p 489 – 492, 2011.

[4] J. Lei, B. Zhou, J. Bian, and X. Q. Jiangsu. *Unit Power Factor Control of PMSM Fed by Indirect Matrix Converter.* 17th International Conference on Electrical Machines and Systems (ICEMS), Hangzhou, China, October 22-25, p.p 926-930, 2014.

[5] T. D. Nguyen and H. H. Lee. *Generalized Carrier-based PWM Method for Indirect Matrix Converters.* 3rd IEEE International Conference on Sustainable Energy Technologies (ICSET), Nepal, pp. 223-228, 2012.

[6] T. D. Nguyen and H. H. Lee. Dual Three-Phase Indirect Matrix Converter With Carrier-Based PWM Method.

IEEE Transactions on Power Electronics, Volume: 29, Issue: 2, pp. 569-581, 2014.

[7] S. M. Dabour, S. M. Allam, and E. M. Rashad. *A Simple CB-PWM Technique for Five-Phase Matrix Converters Including Over-Modulation Mode*. IEEE 8th GCC Conference & Exhibition, Muscat, Oman, February 1-4, P.p 1-6., 2015.

[8] T. D. Nguyen and H. H. Lee. Development of a Three-to-Five-Phase Indirect Matrix Converter with Carrier-Based PWM Based on Space Vector Modulation Analysis. *IEEE Transactions on Industrial Electronics*, Vol. 63, No. 1, pp 13-24, 2016.

[9] J. Rodriguez, M. Rivera, J. W. Kolar, and P. W. Wheeler. A Review of Control and Modulation Methods for Matrix Converters. *IEEE Transactions on Industrial Electronics*, Vol. 59, No. 1, pp 58-70, 2012.

[10] M. Matteini. Control Techniques for Matrix Converter Adjustable Speed Drive. Ph.D. thesis, Department of Electrical Engineering, University of Bologna, 2001.

[11] X. Liu, F. Blaabjerg, P. C. Loh, and P. Wang. *Carrier-based Modulation Strategy and Its Implementation for Indirect Matrix Converter under Unbalanced Grid Voltage Conditions*. 15th International Power Electronics and Motion Control Conference (EPE/PEMC), Europe, Novi Sad, Serbia, pp. LS6a.2-1- LS6a.2-7, 2017.

[12] A. Dieng, M. F. Benkhoris, A. B. Mboup, M. A. Ahmed, J. C. L. Claire1. Analysis of Five-Phase Permanent Magnet Synchronous Motor. _Rev. Roum. Sci. Techn.– Électrotechn. et Énerg_. Vol. 61, No. 2, pp. 116–120, 2016.

[13] L. Parsa. Performance Improvement of Permanent Magnet Ac Motors. Ph.D. Thesis, Department of Electrical Engineering, Texas A&M University, College Station, Texas, 2005.

[14] M. Ahmed. High Performance AC Drives. Springer Berlin Heidelberg, 2010.
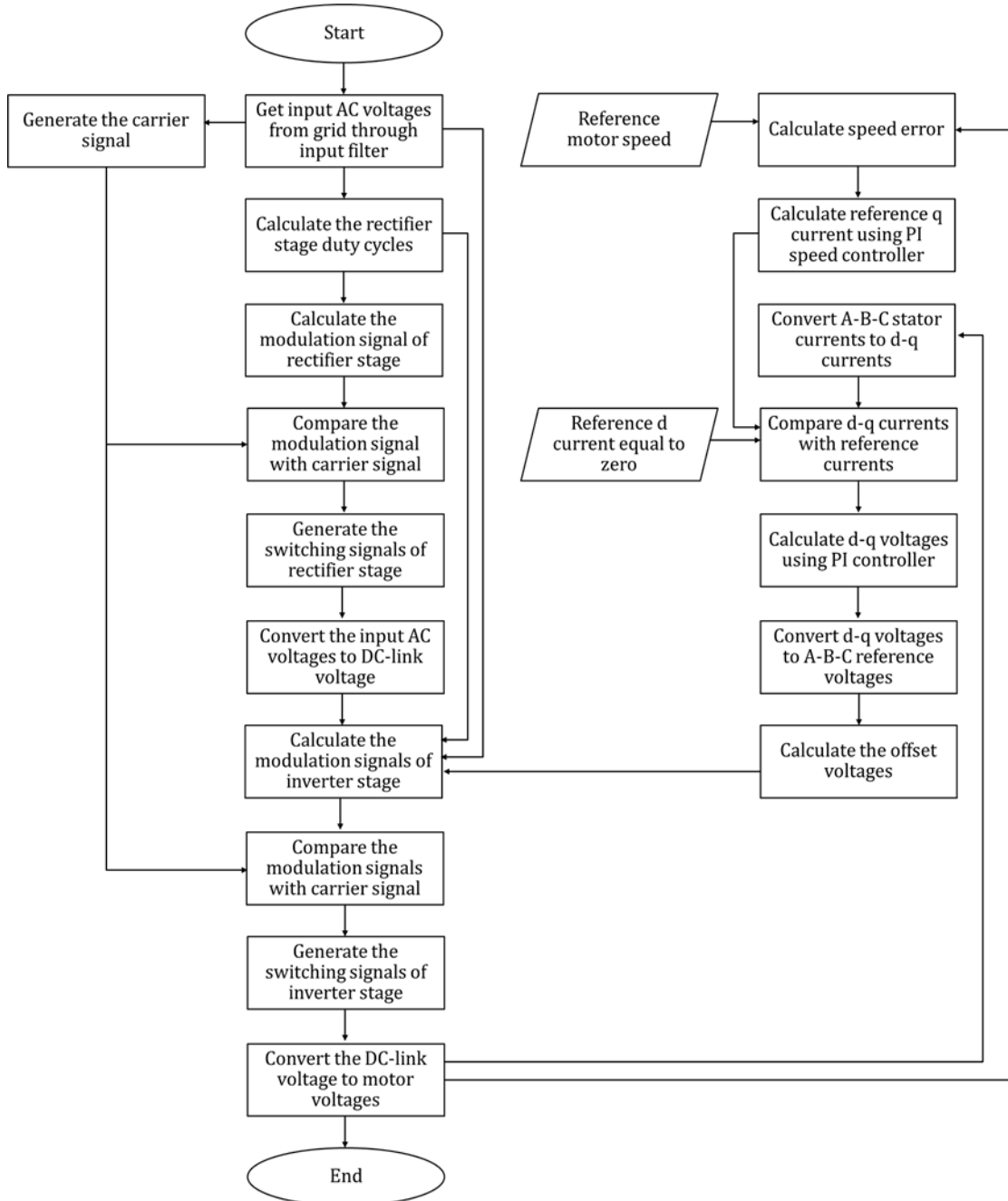
Appendix-A The flowchart of complete Simulink model of proposed system